The Phenomenon of Silicon Plasma Outpacing Air Filamenta-Tion in Tightly Focused Femtosecond Laser Fields

Xian-an Dou *, Xin Li , Qing Ye , Yuntao Xie

Posted Date: 3 February 2025

doi: 10.20944/preprints202502.0144.v1

Keywords: femtosecond laser; filamentation; plasma; ionization thresholds; temporal contrast

 doi:10.20944/preprints202502.0144.v1

Article

The Phenomenon of Silicon Plasma Outpacing Air Filamenta-tion in Tightly Focused Femtosecond Laser Fields

Xian-an Dou[1,2,*], Xin Li[1,2], Qing Ye[1,2], Yuntao Xie[1,2]

[1] State Key Laboratory of Pulsed Power Laser Technology, National University of Defense Technology, Hefei 230037, China

[2] Advanced Laser Technology Laboratory of Anhui Province, Hefei 230037, China

* Correspondence: xian.an_dou@nudt.edu.cn

Abstract: In the field of femtosecond laser physics, a phenomenon has been discovered wherein silicon plasma appears earlier than air filaments in tightly focused femtosecond laser fields. This phenomenon exhibits an advance time of several picoseconds. Analysis of the results reveals that the disparity in ionization thresholds between silicon and the surrounding air is the primary cause of this phenomenon. Moreover, the temporal contrast of the femtosecond laser pulses influences the extent of the advance time. The findings provide valuable insights into the complex interactions between laser-plasma and laser-material interactions, and have implications for advancements in the laser precision machining, laser remote sensing, and related applications.

Keywords: femtosecond laser; filamentation; plasma; ionization thresholds; temporal contrast

1. Introduction

The advent of femtosecond laser technology has revolutionized the field of laser-matter interactions, offering unprecedented insights into the ultrafast dynamics of materials under extreme conditions[1, 2]. Femtosecond lasers, characterized by their sub-picosecond pulse durations, enable the exploration of material responses at timescales that were previously inaccessible[3-6]. This capability has not only expanded our understanding of fundamental physical processes[7, 8] but also paved the way for numerous applications in fields ranging from precision machining to biomedical science[9-14].

One of the most intriguing phenomena associated with femtosecond lasers is the formation of plasma filaments. These filaments arise from the delicate balance between Kerr self-focusing and plasma defocusing, resulting in the propagation of high-intensity light over extended distances[15-17]. Within filaments, a plethora of nonlinear optical effects occur, including intensity clamping[18], supercontinuum generation[19, 20], high harmonic generation[21], THz generation[22], light bullet[23-25], air lasing[26, 27], molecular alignment[16], air birefringence[28], and the induction of water condensation[29]. These diverse effects have spurred numerous ideas for practical applications such as material processing[14], lightning protection[30], weather control[29], atmospheric clearing[31], optical air waveguides[32], and optical communications[33]. However, a comprehensive understanding of the plasma dynamics and laser-material interactions involved in filamentation remains elusive. This study aims to investigate a previously unreported phenomenon of silicon plasma preceding the formation of femtosecond filaments in highly focused laser fields. The objective is to unravel the underlying mechanisms governing this phenomenon and gain a deeper understanding of the associated dynamics. Our findings not only contribute to the fundamental knowledge of laser-matter interactions but also hold potential applications in laser remote sensing, laser beam transmission and control, and laser parameter measurement and regulation.

 doi:10.20944/preprints202502.0144.v1

2. Experiment

To investigate the ultrafast transient behavior of silicon plasma and air filamentation induced by tightly focused femtosecond laser pulses, we employed pump-probe time-resolved shadowgraph imaging. The experimental setup, as depicted in Figure 1, utilized a chirped pulse amplification (CPA) Ti: sapphire laser system (Amplitude Centaurus) to generate 50 fs pulses at a repetition rate of 10 Hz, with a central wavelength of 800nm.

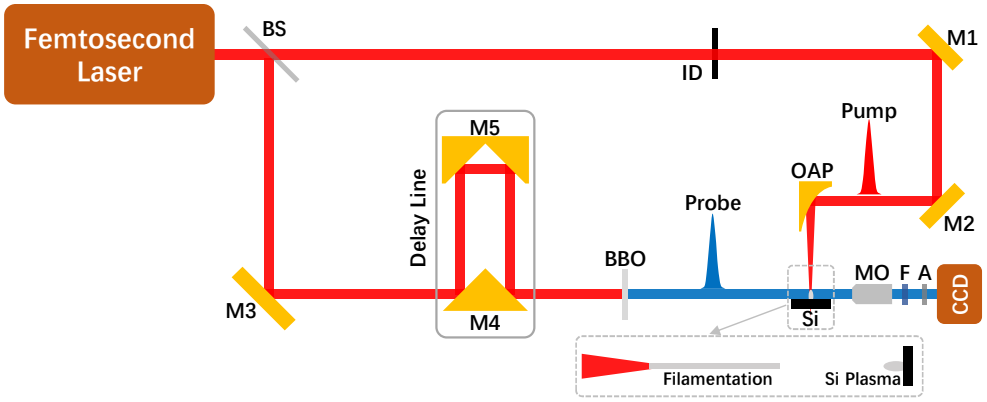

Figure 1. Schematic illustration of the experimental setup for observing the transient behavior of silicon and air in a tightly focused femtosecond laser field. (BS: thin film beam splitter, ID: iris diaphragm, M1-M3: mirrors, M4: 90° specialty mirror, M5: retroreflector, OAP: off-axis parabolic mirrors, MO: microscope objective, F: narrow band filter, A: neutral density filter. The image within the dashed box represents an enlarged view of the focal area.)

The laser beam was split into two beams—the pump and the probe—using a thin-film beamsplitter (Thorlabs BP245B2, R: T = 45%:55%). The pump beam, after passing through the beamsplitter, had its width and pulse energy controlled by an iris diaphragm (Thorlabs ID25Z) and its direction steered by mirrors M1 and M2. It was then focused onto a silicon wafer using an off-axis parabolic mirror (Thorlabs MPD129-G01, f=50.8 mm) at normal incidence to excite the air and silicon, thereby inducing air filamentation and silicon plasma. Meanwhile, the probe beam, reflected by the beamsplitter and M3, was directed through an optical delay line consisting of a stepper motor stage and two reflectors (M4: 90° Specialty Mirror, Edmund #47-239; M5: Gold Retroreflector, Edmund #49-676) to precisely control the laser pulse delay time. The probe beam subsequently passed through a BBO crystal (CASTECH) for second harmonic generation, providing illumination for the air filament and silicon plasma, both of which were parallel to the silicon wafer's surface. To minimize broadening of the femtosecond laser pulses due to optical elements, low-dispersion components were used throughout the experimental setup. To reduce the broadening of femtosecond laser pulses caused by optical elements, low-dispersion components were used throughout the experimental setup. These components included metal-coated optical mirrors (M1-M5 and OAP), an ultra-thin beamsplitter (BS), and a BBO crystal.

The shadow images of the air filament and silicon plasma were synchronously captured using an imaging system composed of a long working distance microscope objective (10× Mitutoyo Plan Apo), a narrow bandpass filter, several neutral density filters, and a CCD camera (Point Grey GS3-U3-28S4M-C, pixel size: 3.69μm). The resolution of the shadow imaging system was evaluated to be 0.9μm/pixel using a resolution test target (Thorlabs R1L3S5P). The image of the resolution test target captured by the imaging system is shown in Figure 2.

 doi:10.20944/preprints202502.0144.v1

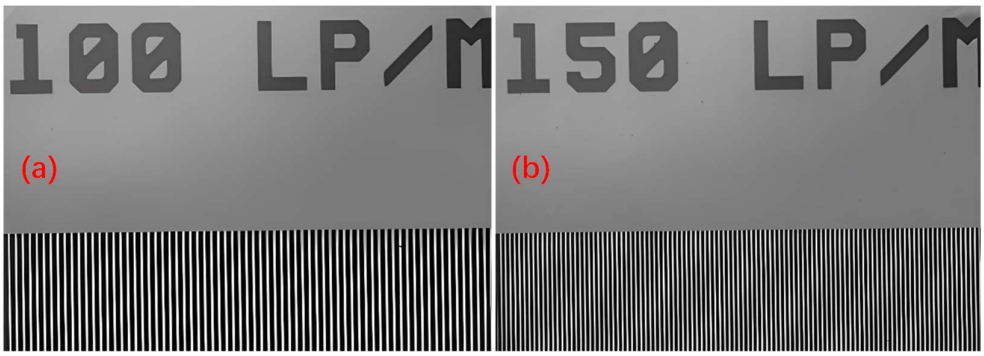

Figure 2. Shadowgraph images of the resolution test target. (a) 100lp/mm; (b)150lp/mm.

The silicon wafer was positioned on the focal plane of the lens, with the pulse energy set to approximately 8.9mJ. The transient evolution of air and silicon ionization in the tightly focused femtosecond laser field was successfully captured using ultrafast time-resolved shadow imaging. To vary the delay time of the probe laser relative to the pump laser, the optical path length of the probe beam was adjusted by driving mirrors M4 and M5 along the beam direction using a high-precision stepper motor stage. This sophisticated setup enabled us to capture transient shadow images of air filaments and silicon plasmas at various delay times, providing a comprehensive visual representation of the observed phenomena, as presented in Figure 3.

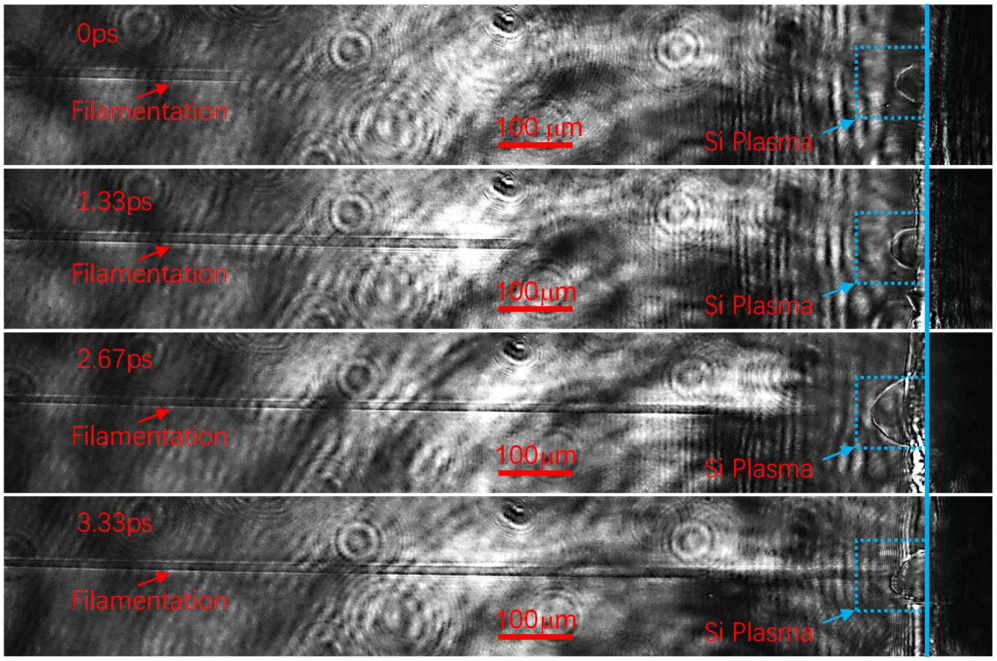

Figure 3. Ultrafast time-resolved shadow images depicting the transient evolution of the air filament and silicon plasma.

In Figure 3, the black region on the right represents the silicon wafer, while the bright gray area on the left corresponds to air. The alternating bright and dark stripes near the surface of the silicon wafer are diffraction patterns at the wafer's edge. The filaments indicated by the red arrow are air filaments, and the semicircular bubbles within the dashed box, pointed to by the blue arrow, represent silicon plasmas.

Typically, in femtosecond laser-matter interactions, the sequence of events is expected to begin with the excitation of an air filament, which then propagates alongside the femtosecond laser pulse

 doi:10.20944/preprints202502.0144.v1

towards the surface of the silicon wafer, culminating in the excitation of silicon plasma. However, our experimental findings reveal a significant deviation from this conventional sequence. Specifically, we observed that the silicon plasma was excited prior to the air filament reaching the surface of the silicon wafer. This unexpected observation suggests that the breakdown of the silicon wafer occurs earlier than that of the air layer situated near its surface, particularly the air spanning from the end of the air filament to the silicon wafer surface. This finding not only provides new insights into the complex interactions between the laser and the material but also challenges the conventional understanding of the excitation sequence in tightly focused femtosecond laser fields.

By conducting a meticulous temporal analysis of the air filament's position across multiple instances, we ascertained that the propagation velocity of the air filament is commensurate with the speed of light. Specifically, the maximum thickness of the air layer was measured to be approximately 900μm, which corresponds to a temporal delay of roughly 3ps between the leading edge of the air filament and the breakdown of the silicon wafer. This substantial temporal disparity not only reveals a compelling facet of our experimental observations but also underscores the necessity for further in-depth investigation.

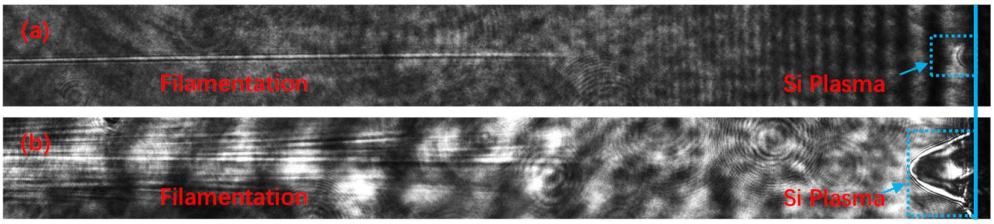

Figure 4. The time-resolved shadow images of the air filament and silicon plasma at different pump energy. (a) 1.8mJ; (b)15.6mJ.

Furthermore, by modulating the pulse energy of the femtosecond laser through adjustment of the iris diaphragm aperture size, we observed changes in the morphology of the air filament and silicon plasma, as illustrated in Figure 4. Specifically, when the pulse energy was reduced to 1.8mJ, the air filament became thinner, and the silicon plasma shrank. Conversely, when the pulse energy was increased to 15.6mJ, the air filament evolved into a multi-filament structure, and the silicon plasma expanded significantly. Despite these morphological changes, the precedence phenomenon remained evident, and the precedence time showed no discernible variation. This suggests that the precedence phenomenon is largely independent of pulse energy variations, indicating that other factors may be influencing this behavior.

3. Discussion

In this section, we delve into the implications of the timing discrepancy observed in the experimental results. The unexpected observation that silicon plasma is excited prior to the air filament challenges the conventional sequence of events in femtosecond laser-matter interactions. This finding provides new insights into the complex interactions between the laser and the material.

Several potential mechanisms have been proposed to explain this phenomenon. Initially, flying focus was considered a plausible explanation[34]. However, upon careful analysis, it was discovered that the experimental phenomenon cannot be explained by the theory of flight focus. Typically, the movement direction of the flight focus remains consistent (either forward or backward). In this experiment, silicon is initially ionized to generate plasma, followed by the subsequent ionization of the air near its surface, suggesting that the focus moves backward. Nevertheless, the propagation direction of the filamentation is forward. This suggests that the ionization processes of the two are independent events.

Cascade ionization may also be the mechanism behind this phenomenon. However, it is important to note that in gases at one atmospheric pressure under femtosecond laser conditions, there

 doi:10.20944/preprints202502.0144.v1

is generally a minimal occurrence of inverse Bremsstrahlung and cascade ionization. This is mainly due to the fact that the mean free time of a free electron released from an atom or molecule through multiphoton/tunnel ionization is longer than the duration of the femtosecond laser pulse itself[15]. These limitations highlight the need to explore alternative mechanisms that could account for the earlier breakdown of the silicon wafer compared to the air layer near its surface.

One potential explanation for the observed phenomenon is the significant difference in ionization thresholds between air and silicon in the femtosecond laser field. Previous studies have established that the ionization threshold for air, when subjected to femtosecond laser pulses, is approximately 50TW/cm²[15]. In contrast, based on experimental data[35], the ionization threshold of silicon is estimated to be around 2.6 TW/cm² for a 50fs laser pulse. The ionization threshold of air is nearly 20 times higher than that of silicon. To further explore this possibility, we conducted an analysis of the spatio-temporal distribution of the optical field generated by the focused femtosecond laser and compared it with the ionization thresholds of both air and silicon.

The intensity of a tightly focused femtosecond laser can be articulated through the following equation:

$$I(z,r,t) = E_0 F_T(z,t) F_S(z,r) \tag{1}$$

Herein, E_0 signifies the pulse energy, $F_T(z,t)$ characterizes the temporal profile, and $F_S(z,r)$ delineates the spatial distribution of the laser. The temporal and spatial profiles are detailed as:

$$F_T(z,t) = \sqrt{\frac{4ln2}{\pi}}\frac{1}{t_p} exp\left(-4ln2\frac{(t-z/c)^2}{t_p^2}\right) \tag{2}$$

and

$$F_S(z,r) = \frac{2}{\pi\omega(z)^2} exp\left(-\frac{2r^2}{\omega(z)^2}\right) \tag{3}$$

In equation (2), t_p denotes the pulse duration, c is the speed of light, and t represents time. In equation (3), r is the transverse spatial coordinate, z is the longitudinal spatial coordinate, and $\omega(z)$ is the radius of the laser beam at position z, which can be determined by:

$$\omega(z)^2 = \omega_0^2 + \left(\frac{\lambda z}{\pi\omega_0}\right)^2 \tag{4}$$

Where λ is the laser wavelength and ω_0 is the radius of the beam waist, calculated as:

$$\omega_0 = \frac{\lambda F}{\pi\omega_l} \tag{5}$$

Here, F is the focal length of the lens, and ω_l is the radius of the laser beam at the front surface of the lens.

Employing a femtosecond laser with a pulse duration of 50fs, a pulse energy of 8.9mJ, and a wavelength of 800nm, we determined that the beam radius at the anterior surface of the lens is 1.5cm, with the lens having a focal length of 5cm. The laser propagates along the positive z-axis within the laboratory reference frame, with the focal plane of the lens defined at z=900μm to facilitate direct comparison with experimental outcomes. Equations (1) through (5) are utilized to ascertain the temporal distribution of light intensity along the optical axis at discrete axial distances z, as depicted in Figure 5(a).

 doi:10.20944/preprints202502.0144.v1

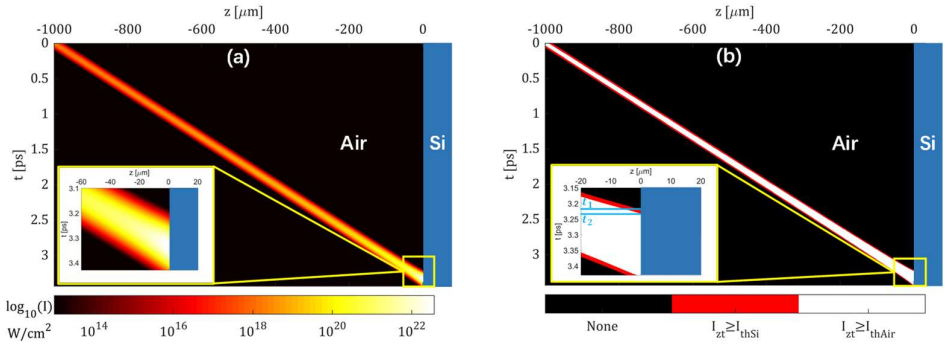

Figure 5. Spatio-temporal distribution of the tightly focused femtosecond laser field and the breakdown region of air and silicon. (a) tightly focused femtosecond laser field. (b) breakdown region of air (white) and silicon (orange plus white).

Figure 5(a) illustrates a pronounced enhancement of light intensity at the focal plane. A comparative analysis of the light intensity with the ionization thresholds for Si and air is conducted, delineating the spatiotemporal regions where the intensity exceeds the Si threshold in red and those surpassing the air threshold in white within Figure 5(b). The lower ionization threshold of Si, as compared to air, results in a more extensive red-marked area, which overlaps with the white-marked region at the center but extends beyond it at the periphery. This distinct pattern reveals that at the focal plane (z = 900μm), the light intensity sequentially surpasses the thresholds of Si and air with the progression of time. Consequently, this sequence initiates the formation of Si plasma prior to the generation of air plasma. The leading edge of the femtosecond laser pulse effectively ablates silicon, thereby initiating silicon plasma formation. In contrast, the higher ionization threshold of air limits ionization to the air molecules in the immediate vicinity of the pulse's peak intensity.

Moreover, the simulation outcomes indicate a lead time that is remarkably brief ($dt=t_2-t_1=12fs$), aligning with the pulse duration and diverging from the experimentally observed several picoseconds. This divergence is likely due to the temporal contrast of the femtosecond laser pulses.

To substantiate the hypothesis regarding the impact of temporal contrast on laser pulses, this investigation takes into account the actual temporal contrast of the laser pulses. For a more accurate depiction of the temporal contrast of laser pulses, the pulse time distribution formula (2) has been refined, yielding formula (6).

$$F_{TC}(z,t) = \sqrt{\frac{4ln2}{\pi}}\frac{1}{t_p}\left[exp\left(-4ln2\frac{\left(t-\frac{z}{c}\right)^2}{t_p^2}\right) + \sum_{i=1}^{4} C_i exp\left(-4ln2\frac{\left(t-\frac{z}{c}\right)^2}{t_{ci}^2}\right)\right] \quad (6)$$

Within the equation, C_i represents the temporal contrast measured at t_{ci}. The calculations have been refined based on the temporal contrast parameters furnished by the laser manufacturer, which are specified as 3×10^{-4} at 1ps, 6×10^{-6} at 5ps, 2×10^{-8} at 20ps, and 5×10^{-10} at 50ps. The modified computational outcomes are illustrated in Figure 6.

 doi:10.20944/preprints202502.0144.v1

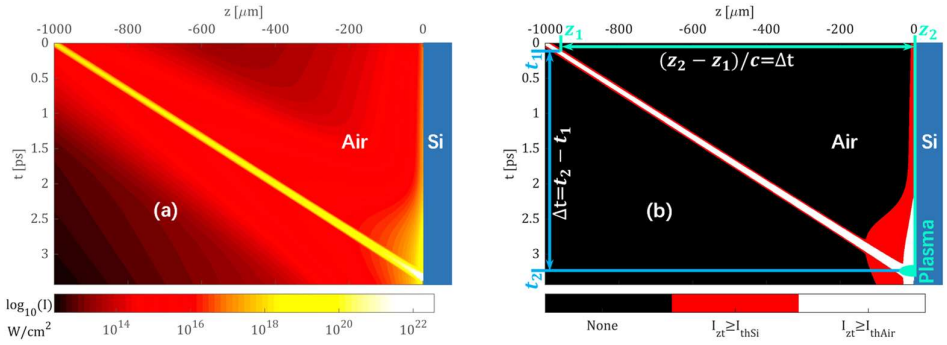

Figure 6. Modified spatio-temporal distribution of the tightly focused femtosecond laser field and the breakdown region of air and silicon. (a) tightly focused femtosecond laser field. (b) breakdown region of air (white) and silicon (orange plus white).

Figure 6(a) elucidates the broadening of the temporal distribution of the leading and trailing edges of the femtosecond laser pulse prior to the focus. At the focal plane, the focusing action of the lens maintains a higher level of intensity over a more extended duration. By comparing the spatiotemporal distribution of the light intensity with the ionization thresholds of Si and air, we delineate the ionization regions for Si and air, as depicted in Figure 6(b). Notably, at t_1=0.12ps, air at z=-960μm and Si at z=0μm can both be ionized to produce plasma, while the intervening air remains un-ionized as the laser intensity has not yet reached the ionization threshold. This indicates that, relative to the air near the Si wafer surface (e.g., at z=-30μm), Si ionizes nearly 3ps earlier. Subsequently, as time progresses and the pulse propagates along the positive z-axis, the region of air ionization gradually approaches the Si wafer, reaching the surface at t_2=3.33ps. These computational results effectively account for the experimental observation of Si plasma preceding air plasma excitation.

The results of the preceding discussion have revealed that the distinct ionization thresholds between silicon and air are primarily responsible for the intriguing phenomenon where silicon plasma forms prior to air filamentation. Furthermore, it has been observed that the temporal contrast of femtosecond laser pulses plays a significant role in determining the lead time of this process.

4. Conclusions

Our study has uncovered a phenomenon whereby silicon plasma emerges before air filaments in tightly focused femtosecond laser fields. We have successfully demonstrated that the disparity in ionization thresholds between silicon and air serves as the primary catalyst for the observed phenomenon, wherein silicon plasma precedes the air filament. Additionally, the temporal contrast of the femtosecond laser noticeably influences the duration of the leading time. These findings contribute to a more nuanced understanding of laser-plasma interactions and may offer value in areas such as laser remote sensing, beam transmission and control, and laser parameters assessment.

Author Contributions: Conceptualization, experiment, validation and original draft preparation, Xian-an Dou; writing—review and editing, Xin Li, Qing Ye and Yuntao Xie. All authors have read and agreed to the published version of the manuscript.

Data Availability Statement: The data presented in this study are available on request from the corresponding author.

Conflicts of Interest: The authors declare no conflict of interest.

 doi:10.20944/preprints202502.0144.v1

References

1. Lamač, M.; Chaulagain, U.; Nejdl, J.; Bulanov, S.V., Generation of intense magnetic wakes by relativistic laser pulses in plasma. *Sci Rep-Uk* **2023**, *13*, (1), 1701.
2. Houard, A.; Walch, P.; Produit, T.; Moreno, V.; Mahieu, B.; Sunjerga, A.; Herkommer, C.; Mostajabi, A.; Andral, U.; André, Y.; Lozano, M.; Bizet, L.; Schroeder, M.C.; Schimmel, G.; Moret, M.; Stanley, M.; Rison, W.A.; Maurice, O.; Esmiller, B.; Michel, K.; Haas, W.; Metzger, T.; Rubinstein, M.; Rachidi, F.; Cooray, V.; Mysyrowicz, A.; Kasparian, J.; Wolf, J., Laser-guided lightning. *Nat Photonics* **2023**, *17*, (3), 231-235.
3. Mishra, Y.N.; Wang, P.; Bauer, F.J.; Zhang, Y.; Hanstorp, D.; Will, S.; Wang, L.V., Single-pulse real-time billion-frames-per-second planar imaging of ultrafast nanoparticle-laser dynamics and temperature in flames. *Light: Science & Applications* **2023**, *12*, (1), 47.
4. Zheng, H.; Yin, F.; Wang, T.; Liu, Y.; Wei, Y.; Zhu, B.; Zhou, K.; Leng, Y., Time-resolved measurements of electron density and plasma diameter of 1 kHz femtosecond laser filament in air. *Chin Opt Lett* **2022**, *20*, (9), 93201.
5. Man, M.K.L.; Margiolakis, A.; Deckoff-Jones, S.; Harada, T.; Wong, E.L.; Krishna, M.B.M.; Madéo, J.; Winchester, A.; Lei, S.; Vajtai, R.; Ajayan, P.M.; Dani, K.M., Imaging the motion of electrons across semiconductor heterojunctions. *Nat Nanotechnol* **2017**, *12*, (1), 36-40.
6. Wolter, B.; Pullen, M.G.; Le, A.T.; Baudisch, M.; Doblhoff-Dier, K.; Senftleben, A.; Hemmer, M.; Schröter, C.D.; Ullrich, J.; Pfeifer, T.; Moshammer, R.; Gräfe, S.; Vendrell, O.; Lin, C.D.; Biegert, J., Ultrafast electron diffraction imaging of bond breaking in di-ionized acetylene. *Science* **2016**, *354*, (6310), 308-312.
7. Sharma, A., High Energy electron and proton acceleration by circularly polarized laser pulse from near critical density hydrogen gas target. *Sci Rep-Uk* **2018**, *8*, (1), 2191.
8. Yamanouchi, K.; Charalambidis, D., *Progress in Ultrafast Intense Laser Science XV*. Springer Nature: Cham, 2020; Vol. 136.
9. Li, Z.; Lin, J.; Wang, C.; Li, K.; Jia, X.; Wang, C.; Duan, J.A., Damage performance of alumina ceramic by femtosecond laser induced air filamentation. *Optics & Laser Technology* **2025**, *181*, 111781.
10. Pimenov, S.M.; Zavedeev, E.V.; Arutyunyan, N.R.; Jaeggi, B.; Neuenschwander, B., Femtosecond laser-induced periodic surface structures on diamond-like nanocomposite films. *Diam Relat Mater* **2022**, *130*, 109517.
11. Tsibidis, G.D.; Mansour, D.; Stratakis, E., Damage threshold evaluation of thin metallic films exposed to femtosecond laser pulses: The role of material thickness. *Optics & Laser Technology* **2022**, *156*, 108484.
12. ZOU, G.; YE, J.; BAO, X., Observation on the clinical effect of femtosecond laser small incision lens extraction in the correction of myopia and astigmatism. *Minerva Surg* **2022**, *77*, (6), 610-612.
13. Kryszak, B.; Szustakiewicz, K.; Dzienny, P.; Junka, A.; Paleczny, J.; Szymczyk-Ziółkowska, P.; Hoppe, V.; Antończak, A., Functionalization of the PLLA surface with a femtosecond laser: Tailored substrate properties for cellular response. *Polym Test* **2022**, *116*, 107815.
14. Wang, D.; Xin, C.; Yang, L.; Wang, L.; Liu, B.; Wu, H.; Wang, C.; Pan, D.; Ren, Z.; Hu, Y.; Li, J.; Chu, J.; Wu, D., Femtosecond Laser Fabrication of Three-Dimensional Bubble-Propelled Microrotors for Multicomponent Mechanical Transmission. *Nano Lett* **2024**, *24*, (10), 3176-3185.
15. Chin, S.L., *Femtosecond Laser Filamentation*. Springer: New York, 2010.
16. Chin, S.L.; Xu, H., Tunnel ionization, population trapping, filamentation and applications. *Journal of Physics B: Atomic, Molecular and Optical Physics* **2016**, *49*, (22), 222003.
17. Peña, J.; Reyes, D.; Richardson, M., Filamentation in low pressure conditions. *Sci Rep-Uk* **2022**, *12*, (1), 21365.
18. Harilal, S.S.; Yeak, J.; Phillips, M.C., Plasma temperature clamping in filamentation laser induced breakdown spectroscopy. *Opt Express* **2015**, *23*, (21), 27113.
19. Liu, Y.; Yin, F.; Wang, T.; Leng, Y.; Li, R.; Xu, Z.; Chin, S.L., Stable, intense supercontinuum light generation at 1 kHz by electric field assisted femtosecond laser filamentation in air. *Light: Science & Applications* **2024**, *13*, (1), 42.
20. Geints, Y.E.; Bulygin, A.D.; Kompanets, V.O.; Chekalin, S.V., Supercontinuum saturation of a femtosecond laser filament in pressurized gases. *Opt Lett* **2024**, *49*, (21), 6033.
21. Li, D.; Hao, Z.; Li, J.; Cai, Y.; Zhang, L., Polarization of the third harmonic emission from the filamentation of femtosecond cylindrical vector beams. *Opt Express* **2024**, *32*, (1), 387.

22. Babushkin, P.A.; Bulygin, A.D.; Geints, Y.E.; Kabanov, A.M.; Oshlakov, V.K.; Petrov, A.V.; Khoroshaeva, E.E., Turbulence-enhanced THz generation by multiple chaotically-distributed femtosecond filaments in air. *Optics & Laser Technology* **2024**, *179*, 111322.
23. Pushkarev, D.V.; Zhidovtsev, N.A.; Uryupina, D.S.; Mitina, E.V.; Volkov, R.V.; Savel Ev, A.B., Three-domain stabilization of femtosecond filament red-shifted light bullet in air by means of beam amplitude modulation. *Optics & Laser Technology* **2025**, *180*, 111438.
24. Brée, C.; Babushkin, I.; Morgner, U.; Demircan, A., Regularizing Aperiodic Cycles of Resonant Radiation in Filament Light Bullets. *Phys Rev Lett* **2017**, *118*, (16), 163901.
25. Panagiotopoulos, P.; Whalen, P.; Kolesik, M.; Moloney, J.V., Super high power mid-infrared femtosecond light bullet. *Nat Photonics* **2015**, *9*, (8), 543-548.
26. Mei, H.; Jiang, H.; Houard, A.; Tikhonchuk, V.; Oliva, E.; Mysyrowicz, A.; Gong, Q.; Wu, C.; Liu, Y., Fluorescence and lasing of neutral nitrogen molecules inside femtosecond laser filaments in air: mechanism and applications. *Physical Chemistry Chemical Physics : PCCP* **2024**, *26*, (36), 23528-23543.
27. Zeng, T.; Li, N.; Yi, Y., Spatial distribution of self-seeded air lasers induced by the femtosecond laser filament plasma. *J Plasma Phys* **2024**, *90*, (4), 905900404.
28. Yuan, S.; Li, M.; Feng, Y.; Li, H.; Zheng, L.; Chin, S.L.; Zeng, H., Filament-induced ultrafast birefringence in gases. *Journal of Physics. B, Atomic, Molecular, and Optical Physics* **2015**, *48*, (9), 94018-10.
29. Wolf, J.P., Short-pulse lasers for weather control. *Rep Prog Phys* **2018**, *81*, (2), 026001.
30. Fu, S.; Arantchouk, L.; Lozano, M.; Mysyrowicz, A.; Couairon, A.; Houard, A., Laguerre–Gaussian laser filamentation for the control of electric discharges in air. *Opt Lett* **2024**, *49*, (13), 3540.
31. Latty, K.S.; Hartig, K.C., Atmospheric clearing of solid-particle debris using femtosecond filaments. *Phys Rev Appl* **2024**, *22*, (1), 014075.
32. Fu, S.; Mahieu, B.; Mysyrowicz, A.; Houard, A., Femtosecond filamentation of optical vortices for the generation of optical air waveguides. *Opt Lett* **2022**, *47*, (19), 5228-5231.
33. Li, D.; Yan, B.; Yuan, Y.; Cai, Y.; Hao, Z.; Li, J., Real-Time Demonstration of Multi-Gigabit/s Free- Space Optical Communications Employing Femtosecond Laser Filaments in Complex Environment. *J Lightwave Technol* **2024**, *42*, (13), 4402-4409.
34. Froula, D.H.; Turnbull, D.; Davies, A.S.; Kessler, T.J.; Haberberger, D.; Palastro, J.P.; Bahk, S.; Begishev, I.A.; Boni, R.; Bucht, S.; Katz, J.; Shaw, J.L., Spatiotemporal control of laser intensity. *Nat Photonics* **2018**, *12*, 262–265.
35. Liu, X.; Cheng, W.; Petrarca, M.; Polynkin, P., Universal threshold for femtosecond laser ablation with oblique illumination. *Appl Phys Lett* **2016**, *109*, (16), 161604.